SIMULTANEOUS DETERMINATION OF AEROSOL SIZE DISTRIBUTION AND REFRACTIVE INDEX AND SURFACE ALBEDO FROM RADIANCE—PART III: PARAMETRIZATION AND APPLICATION

Qiu Jinhuan (邱金桓)

Institute of Atmospheric Physics, Academia Sinica, Beijing

Received March 15, 1987

ABSTRACT

Based on the radiative transfer calculation results, three approximate expressions of the sky radiance in almucantar and its increment caused by surface albedo are presented. They are simple, but accurate enough. The dependence of the fitted aerosol scattering phase functions on refractive index is also studied, and its reasonable form is given. For Junge size distribution, the approximate equations of the phase functions with some special scattering angles are obtained. These approximate equations significantly simplify the retrieval algorithm of simultaneous determination of aerosol size distribution and its refractive index and surface albedo. This method can be realized with a microcomputer, and has been used to process and analyse the experimental data measured in Hefei of Anhui Province.

I. INTRODUCTION

An optimum remote sensing method should be reasonable in principle, simple and economical in experiment, convenient and rapid in computation. In our theoretical analysis (Qiu and Zhou, 1986), we have proposed a new method for simultaneous determination of aerosol size distribution, and its refractive index and surface albedo from the sky radiance data, and discussed its validity in principle. Based on this theoretical analysis, we have retrieved the aerosol size distribution, and its wavelength-dependent refractive index and surface albedo by use of the sky radiance data in almucantar measured by a multiple-wavelength radiometer (Qiu and Zhou, 1986). This experiment is very simple and economical and the primary experimental results are basically reasonable. But this method is complex and tedious in calculation. In order to retrieve a set of data, we must solve the radiative transfer equation for more than five times by using a larger computer. In this paper, with the numerical solution of the radiative transfer equation under different aerosol optical property and surface albedo, we obtain a few of approximate expressions about the sky radiance and the scattering phase functions. Hence the computational process is simplified greatly.

II. APPROXIMATE EXPRESSIONS

1. *The Sky Radiances at about* 40° *and* 90°

According to the radiative transfer calculation results, when surface albedo (marked

as A) is zero, the sky radiance in almucantar near 40° can be approximately expressed as follows:

$$\begin{cases} B_{40}=\dfrac{\pi F_0 R_M(\theta)}{\mu_0}e^{-\tau_T/\mu_0}[\tau_m P_m(\theta)+\tau_a P_a(\theta)], \\ R_M(\theta)=1+1.2\tau_m/\mu_0^{0.15}+0.72\tau_m^4\tau_{as}/\mu_0^3+0.23\tilde{\omega}g^{0.5}\times \\ \qquad (\tau_{as}+0.6\tau_{as}^3+10\tau_m^3\tau_{as}^3)/(\mu_0^{0.75}+0.65\mu_0^3)/P(\theta), \\ \tau_{as}=\tilde{\omega}_a\tau_a, \end{cases} \tag{1}$$

where θ is the scattering angle and $\mu_0=\cos\alpha$, α being the solar zenith angle; τ_a and τ_m are aerosol and molecular optical depth, τ_T is total optical depth; πF_0 is the extraterrestrial solar spectral irradiance; $P(\theta)$ and $\tilde{\omega}$ are the atmospheric scattering phase function and its single-scattering albedo, $P_a(\theta)$ and $\tilde{\omega}_a$ are the aerosol scattering phase function and its single-scattering albedo, respectively; $P_m(\theta)$ is the molecular scattering phase function; g is an asymmetric factor. $P(\theta)$ and $\tilde{\omega}$ can be expressed as follows:

$$P(\theta)=[\tau_m P_m(\theta)+\tau_a P_a(\theta)]/\tau_T,$$
$$\tilde{\omega}=(\tau_m+\tau_a\tilde{\omega}_a)/\tau_T.$$

While the sky radiance for $\theta=90°$ and $A=0$ in almucantar can be approximately formulated as follows:

$$\begin{cases} B_{90}=\dfrac{\pi F_0 R_M(\theta)}{\mu_0}e^{-\tau_T/\mu_0}[\tau_m P_m(\theta)+\tau_a P_a(\theta)], \\ R_M(\theta)=1+0.0158(1+0.9g)\tilde{\omega}(11\tau_{ss}^{2.78}+4.5\tau_{ss}^{1.5})/ \\ \qquad [\mu_0^{0.25+0.17\tau_{ss}}+2.33\mu_0^3 g^{1.5}-13\tau_{ss}^{1.5}\mu_0^4/(1+2g)^5]/P^{0.6}(\theta), \\ \tau_{ss}=\tau_m+\tau_{as}. \end{cases} \tag{2}$$

Now we consider the relative errors of Eqs. (1) and (2), denoted as E_{40} and E_{90} respectively, *i. e.*

$$E_{40}=|1-B_{40}(\theta=40°)|/B(\theta=40°)\%, \tag{3}$$
$$E_{90}=|1-B_{90}(\theta=90°)|/B(\theta=90°)\%, \tag{4}$$

where the sky radiance $B(\theta)$ is obtained from the numerical solutions of radiative transfer equation, being taken as the exact value.

Table 1 shows the values of E_{40} for Junge distribution with $\nu^*=3$; and $0\leqslant m_I\leqslant 0.05$ and $1.45\leqslant m_R\leqslant 2.1$; and $0.3131\leqslant\mu_0\leqslant 0.8732$; and $0.008\leqslant\tau_m<0.349$ ($0.33\mu m\leqslant\lambda\leqslant 1.013\ \mu$m); and $0.02\leqslant\tau_a\leqslant 0.6$. Here m_R and m_I are the real part and the imaginary part of aerosol refractive index, respectively. As shown in Table 1, the maximum value of E_{40} is less than 5.5%, but the error increases with increasing τ_T. Also when $\tau_a=0.02$, the maximum error is not more than 1.4%, and the average 0.7%. Even if $\tau_a=0.6$, mean value of the errors is not more than 2.9%.

Table 2 shows the values of E_{90} under same conditions as in Table 1. It is found that the maximum of E_{90} is less than 9.0%, and in particular the error decreases when τ_a is small. For example, when $\tau_a\leqslant 0.2$, the maximum error is less than 2.3%, and the average 1.4%.

Table 3 shows the values of E_{40} and E_{90} under different aerosol size distributions. In Table 3, DL and DM represent continental and marine Diermendjian distributions, respectively. For Junge distributions with $\nu^*=2$ and 4, and DL and DM distributions, the values of E_{40} and E_{90} are basically same as for those Junge distribution with $\nu^*=3$

as shown in Tables 1 and 2. For non-Junge distribution, the errors are slightly larger, when $\tau_a \leqslant 0.6$, $E_{40} \leqslant 7.8\%$ and $E_{90} \leqslant 7.3\%$. However when τ_a is smaller, the errors are smaller. For example, when $\tau_a \leqslant 0.2$, E_{40} and E_{90} are less than 3% and 2%, respectively.

Fig. 1 shows the variation of E_{90} and E_{40} with θ. As θ deviates from 40°, E_{40} increases, but when τ_T is smaller, the increase in E_{40} is not obvious. Therefore, the Eq. (1) can be used within $\theta = 40° \pm 5°$. Similarly within $\theta = 90° \pm 10°$, the variation in E_{90} is not evident, and the Eq. (2) is valid.

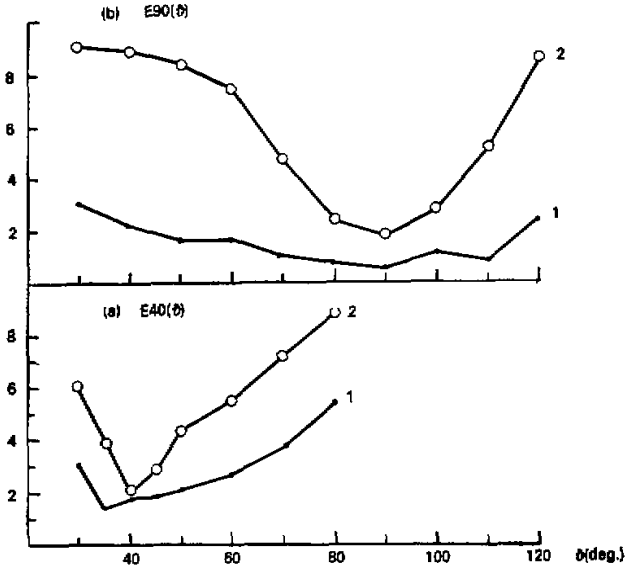

Fig. 1. The variation of E_{40} and E_{90} with θ for $\nu^*=3$, $\tau_m=0.0915$, $\mu_0=0.4617$ and $m=1.5-0.01i$. 1. $\tau_a=0.1$; 2. $\tau_a=0.6$.

Table 1. The Values of E_{40} for Junge Distribution with $\nu^*=3$

μ_0 \ τ_a	0.02	0.1	0.2	0.3	0.4	0.6	τ_m	m
0.3131	1.2	2.8	3.1	2.2	2.5	4.2	0.03538	1.5-0i
0.4617	0.9	2.4	3.0	3.1	3.8	2.7	0.03538	1.5-0i
0.6869	0.5	1.0	1.2	1.5	2.4	2.0	0.03538	1.5-0i
0.8732	0.3	0.4	0.6	2.3	1.0	1.4	0.03538	1.5-0i
0.3131	1.0	2.3	2.0	2.2	2.7	4.0	0.0915	1.5-0.01i
0.4617	1.4	1.9	2.1	1.8	4.0	2.6	0.0915	1.5-0.01i
0.6869	0.1	0.7	1.8	1.8	3.2	4.5	0.0915	1.5-0.01i
0.8732	0.4	1.1	0.8	0.4	0.7	1.8	0.0915	1.5-0.01i
0.3131	1.1	2.1	4.0	3.6	4.8	5.4	0.349	1.5-0.01i

μ_0 \ τ_a	0.02	0.1	0.2	0.3	0.4	0.6	τ_m	m
0.4617	0.9	1.9	1.6	1.7	2.3	1.6	0.349	1.5-0.01i
0.6869	0.5	0.9	1.6	1.5	1.8	1.2	0.349	1.5-0.01i
0.8732	0.8	1.3	1.4	1.2	1.3	1.6	0.349	1.5-0.01i
0.4617	1.1	2.7	3.0	2.3	2.5	2.4	0.03538	1.5-0.01i
0.4617	0.1	1.1	0.3	0.1	0.5	2.2	0.008	1.5-0.01i
0.4617	0.4	1.6	0.5	1.2	2.3	3.5	0.0915	2.1-0i
0.4617	0.5	1.0	0.7	1.8	2.2	3.7	0.0915	1.55-0.01i
0.4617	0.9	1.5	1.9	1.4	2.8	4.1	0.0915	1.45-0.01i
Average	0.7	1.6	1.7	1.8	2.4	2.9		

Table 2. The Values of E_γ for Junge Distribution with $\gamma^*=3$

μ_0 \ τ_a	0.02	0.1	0.2	0.3	0.4	0.6	τ_m	m
0.3131	0.0	0.2	1.1	0.1	1.0	2.6	0.03538	1.5-0i
0.4617	0.3	0.8	1.3	1.6	2.2	3.0	0.03538	1.5-0i
0.6869	0.8	1.2	1.9	1.5	0.3	4.2	0.03538	1.5-0i
0.3131	1.1	1.7	2.2	4.7	6.6	8.9	0.0915	1.5-0.01i
0.4617	0.6	1.2	1.8	3.8	5.0	6.3	0.0915	1.5-0.01i
0.6869	0.6	1.0	1.3	3.2	3.5	4.1	0.0915	1.5-0.01i
0.3131	0.4	0.8	2.3	1.4	2.3	3.5	0.349	1.5-0.01i
0.4617	0.8	1.2	0.5	0.5	0.3	0.8	0.349	1.5-0.01i
0.6869	1.2	1.7	1.0	0.2	1.3	2.4	0.349	1.5-0.01i
0.4617	0.5	0.3	1.6	3.1	2.2	1.9	0.349	1.5-0.01i
0.4617	0.7	1.0	0.3	2.1	2.7	3.6	0.349	1.5-0.05i
0.4617	1.3	1.3	1.8	1.9	3.1	1.8	0.0915	2.1-0i
0.4617	1.4	2.2	1.7	1.6	3.2	5.3	0.0915	1.55-0.01i
0.4617	0.5	0.7	1.3	2.0	2.7	3.4	0.0915	1.45-0.01i
Average	0.6	1.3	1.4	2.0	2.6	3.7		

Table 3. The Values of E_{40} and E_{90} under Different Aerosol Size Distributions

Distribution \ τ_a	0.1		0.2		0.4		0.6		τ_m	μ_0	m
	E_{40}	E_{90}	E_{40}	E_{90}	E_{40}	E_{90}	E_{40}	E_{90}			
$\nu^*=2$	1.2	1.0	2.8	1.8	3.3	1.2	1.5	3.5	0.349	0.3131	1.5-0.02i
$\nu^*=2$	0.9	2.2	1.3	1.9	0.6	2.4	0.2	2.3	0.349	0.6869	1.5-0.02i
$\nu^*=4$	2.0	1.1	1.9	1.0	2.2	3.3	4.0	5.9	0.3	0.6869	1.5-0i
$\nu^*=4$	2.2	1.9	2.8	1.5	4.9	1.4	6.3	5.1	0.1	0.6869	1.5-0i
DL	2.5	0.2	2.2	0.1	1.8	1.9	4.1	6.7	0.3	0.3131	1.5-0i
DL	2.2	1.0	2.4	1.5	4.0	5.1	4.8	7.3	0.3	0.6869	1.5-0i
DL	2.9	1.1	3.6	0.2	6.4	0.8	7.8	4.5	0.0354	0.3131	1.5-0i
DL	1.7	1.7	3.0	1.4	4.5	0.8	6.1	2.3	0.0354	0.6869	1.5-0.05i
DM	2.4	1.6	2.4	1.3	3.2	0.7	5.7	3.8	0.1	0.4617	1.5-0.01i
DM	1.9	1.8	2.3	2.0	4.1	2.2	5.3	4.7	0.1	0.4617	1.6-0.01i

2. *The Increment of the Sky Radiance Caused by Surface Albedo*

Box and Deepak (1981) have pointed out that the increment of the radiance in the same almucantar caused by the albedo for Lambert surface is independent of scattering angle. Furthermore, they have fitted an approximate equation as follows:

$$\begin{cases} \Delta B=\pi F_0\exp(-\tau_T/\mu_0)\tau_A P_m(0^\circ), \\ \tau_A=A\tau_2/(1-A\tau_3), \\ \tau_2=1.34\tau_{ss}\mu_0[1.0+0.22(\tau_{ss}/\mu_0)^2], \\ \tau_3=0.9\tau_{ss}-0.92\tau_{ss}^2+0.54\tau_{ss}^3. \end{cases} \tag{5}$$

This formula has larger error under some condition. In the following we propose an approximate equation with higher accuracy:

$$\begin{cases} \Delta B=\pi F_0\exp(-\tau_T/\mu_0)f_A/\mu_0 \\ f_A=A\tau_2/(1-A\tau_3) \\ \tau_2=0.1648(1-g)^{0.7}\tau_{ss}\mu_0^{0.1}[1+0.36(\tau_{ss}/\mu_0)^2 \\ \qquad +0.8g\tau_{ss}^4\mu_0^2-0.00135/\mu_0^6/(1+g)^6]P^{0.1}(\theta=180^\circ), \\ \tau_3=0.9\tau_{ss}-0.92\tau_{ss}^2+0.54\tau_{ss}^3, \\ P(\theta=180^\circ)=[\tau_m P_m(180^\circ)+\tau_a P_a(180^\circ)]/\tau_T. \end{cases} \tag{6}$$

A comparison of the accuracies of Eqs. (5) and (6) is shown in Tables 4 and 5, where ER_1 and ER_2 are the relative errors of Eqs. (6) and (5), respectively. In Table 4, the difference between the sky radiance for the surface albedo $A=0.25$ and that for $A=0$ is obtained from Box and Deepak's numerical solution of radiative transfer equation, being taken as the exact value of ΔB. For the solar zenith angles of $\alpha=30^\circ$, 45° and 60°, the errors of Eq. (5) are up to 69%. The smaller the solar zenith angle is, the larger τ_T is, and thus the larger the error is. Mean value of 9 sets of errors is 37.1%. But the maximum error of Eq. (6) is not more than 5.6%, and the average 3.4%. They are of one order of magnitude smaller than those of Eq. (5).

In Table 5 we further compare the accuracies of Eqs. (6) and (5) under different aerosol size distributions and refractive indices and different optical depths and solar zenith angles. For Junge distributions with $\nu^*=3$ and 4 and DL distribution, $0.3131\leqslant\mu_0\leqslant0.8732$, $0.03538\leqslant\tau_m\leqslant0.3$, $0.1\leqslant\tau_a\leqslant0.6$, $0\leqslant m_I\leqslant0.05$, and $A=0.2$, the error of Eq. (6) is not more than 6.1% with satisfactory accuracy. But the error of Eq. (5) can be up to 156.6%. Also the smaller μ_0 and τ_m are and the larger τ_a is, the larger the error of Eq. (5) is. However, the error of Eq. (6) is generally less than 6%.

Table 4. Comparison of ER_1 and ER_2

α	30°			45°			60°		
τ_m	0.1	0.1	0.2	0.1	0.1	0.2	0.1	0.1	0.2
τ_a	0.1	0.2	0.1	0.1	0.2	0.1	0.1	0.2	0.1
ER_1	0.4	2.3	5.6	2.1	2.1	5.6	5.5	2.4	4.8
ER_2	47.1	69.0	23.0	40.7	56.8	15.2	30.1	38.5	13.8

Table 5. Comparison of ER_1 and ER_2 under Different Aerosol Optical Properties and Solar Zenith Angles

τ_a / μ_0	0.1		0.2		0.4		0.6		τ_m	m	Distribution
	ER_1	ER_2	ER_1	ER_2	ER_1	ER_2	ER_1	ER_2			
0.3131	4.4	22.4	2.3	27.2	1.8	32.5	1.2	35.3	0.0915	1.5-0.01i	$\nu^*=3$
0.4617	1.7	42.9	4.0	48.9	3.4	54.7	5.4	58.0	0.0915	1.5-0.01i	$\nu^*=3$
0.6869	4.0	67.0	3.2	74.5	3.4	81.5	1.0	85.0	0.0915	1.5-0.01i	$\nu^*=3$
0.8732	1.6	84.5	2.0	91.6	4.8	99.6	3.9	103.5	0.0915	1.5-0.01i	$\nu^*=3$
0.6869	1.2	87.4	1.7	110.0	3.1	115.2	2.2	112.4	0.03538	1.5-0.01i	$\nu^*=3$
0.6869	4.0	70.4	3.7	100.8	3.2	135.6	6.1	156.6	0.03538	1.5-0.05i	$\nu^*=3$
0.6869	2.0	64.1	3.2	78.4	2.8	80.0	3.7	79.4	0.03538	1.5-0.01i	$\nu^*=4$
0.6869	1.6	12.8	2.1	20.1	2.6	28.9	4.9	30.5	0.3	1.5-0i	DL

3. *The Scattering Phase Function*

In order to accurately determine aerosol refractive index and surface albedo, the scattering phase functions with $\theta=10°$, 40°, 90° and 180° should be given. However, the phase function is complicatedly dependent on aerosol size distribution and its refractive index. Tanaka et al. (1982) retrieved refractive index from the phase functions by using the library method. In their paper, 30 grid points in the range of $0.004\leqslant m_I\leqslant0.08$ and $1.45\leqslant m_R\leqslant1.65$ are taken. Analyzing the dependence of aerosol phase function on refractive index, we find that under the condition that $0\leqslant m_I\leqslant0.1$, the scattering phase functions for all angles are rather in accordance with the following form:

$$\begin{cases} P_a(\theta,m_R,m_I)=P_a(\theta,m_R,m_I=0)+a_1 m_I^{(1+10.9\xi^{0.8}+a_2 m_I^{1.7})}, \\ E=1-P(\theta,m_R,m_I=0.03)/P(\theta,m_R,m_I=0), \end{cases} \tag{7}$$

where a_1 and a_2 are the parameters which are relative to aerosol size distribution and refractive index. For arbitrary size distribution and the real part of refractive index, as long as three values of m_I are chosen, E, a_1 and a_2 can be determined. Hence the phase function with arbitrary imaginary part of refractive index can be determined. In this paper, $m_I=0$, 0.03 and 0.08 are taken as grid points. Fig. 2 shows the relative errors of the phase functions determined by (7), marked as $E_P(\theta)$. For Junge distributions with $\nu^*=2$, 3 and 4, and DL and DM distributions, $m_R=1.45$ and 1.6, $0\leqslant m_I\leqslant 0.1$, the error of phase function at $\theta=40$ is less than 3%. Table 6 shows the maximum values of $E_P(\theta)$ under the conditions of the above-mentioned five distributions and $m_R=1.4$, 1.45, 1.5, 1.55 and 1.6 and $0\leqslant m_I\leqslant 0.08$.

As shown in Table 6, for $\theta=10°$, 40° and 90°, the maximum errors are less than 2%, but for $\theta=180°$, the maximum error is slightly larger, and in particular for Junge distribution with $\nu^*=2$ having a lot of large particulates, the maximum error may be up to 14.2%.

Table 6. The Error in Eq. (7) for Different Scattering Angles

Distribution \ θ	10°	40°	90°	140°	180°
$\nu^*=2$	1.7	1.2	1.5	2.1	14.2
$\nu^*=3$	1.1	0.6	0.5	1.5	5.4
$\nu^*=4$	0.8	1.0	1.6	3.7	2.9
DL	1.3	1.1	1.9	2.8	6.2
DM	1.8	1.5	1.7	3.1	7.4

Furthermore, the dependence of the phase functions for $\theta=10°$, 40°, 90° and 180° on the real part of refractive index can be given approximately:

$$P_a(\theta,m_R,m_I)=P_a(\theta,m_R=1.54,m_I=0)\left(\frac{m_R}{1.54}\right)^{c_0}f(m_R)$$

$$+a_{10}\left(\frac{m_R}{1.54}\right)^{c_1}m_I\left[1+10.9E^{0.8}m_I+a_{20}\left(\frac{m_R}{1.54}\right)^{c_2}m_I^{1.1}\right], \qquad (8)$$

$$E=E_0\left(\frac{m_R}{1.54}\right)^{c_3}$$

$$f(m_R)=\begin{cases}1, & \text{for } \theta=10°,\\ \sin(m_R), & \text{for } \theta=40°,\\ \sin(0.84m_R), & \text{for } \theta=90°,\\ 1, & \text{for } \theta=180°.\end{cases}$$

In the range of $1.4\leqslant m_R\leqslant 1.65$ and $0\leqslant m_I\leqslant 0.1$, $m_R=1.48$ and 1.54 and $m_I=0$, 0.03 and 0.08 can be chosen as grid prints. Thus c_0, a_{10}, c_1, a_{20}, c_2 and c_3 in Eq. (8) can be determined. For instance, a_2 can be determined by using following iterative algorithm:

$$a_2^{(0)}=0$$

$$a_1^{(1)}=[P_a(\theta,m_R,m_I=0.03)-P_a(\theta,m_R,m_I=0)]/m_I^{(1+10.9E^{0.8}m_I)},$$
$$a_2^{(1)}=\ln\{[P_a(\theta,m_R,m_I=0.08)-P_a(\theta,m_R,m_I=0)]/m_I^{(1+10.9E^{0.8}m_I)}a_1^{(1)}\}/\ln(0.08)/0.08^{1.7}.$$

For general aerosol size distribution, and $1.45\leqslant m_R\leqslant 1.65$, $0\leqslant m_I\leqslant 0.08$, the errors of phase functions at $\theta=10°$, 40° and 90° determined by (8) are less than 3%, and the error at $\theta=180°$ is less than 35%. The increment of radiance in almucantar caused by surface albedo is approximately proportional to $P^{0.1}(180°)$, being insensitive to the error of the phase functions at $\theta=180°$, 40% error in the phase function only causes 3.4% error in the absolute increment of the sky radiance. The accuracy of Eq. (8) is accurate enough.

For Junge distribution, the phase function at $\theta=40°$ can be further parameterized as follows:

$$\begin{cases} P_a(40°,m_I,m_R)=(0.074\nu^{*2.5}+0.048\nu^{*}-0.008\nu^{*2}-0.034)[\sin(m_R)]^{(8-0.5\nu^{*})} \\ \qquad -(3.4+0.008\exp(\nu^{*1.4})m_R^{(4-2\nu^{*})}m_I^{(1+10.9E^{0.8}}m_I+a_2m_I^{1.7}), \\ E=(0.184+3.13\nu^{*-1}+2.44\times10^{-4}\nu^{*7}-0.85\times10^{-4}\nu^{*6})m_R^{(2.5-1.5\nu^{*})}, \\ a_2=-0.4m_R^2-0.6(\nu^{*2}-6\nu^{*}+9) \end{cases} \quad (9)$$

For non-Junge distribution, so long as ν^* in Eq. (9) is replaced by equivalent Junge distribution parameter determined from Eq. (10), the Eq. (9) still holds. Table 7 shows an example about this. In Table 7, P_a is the real phase function, and P_a^{**} is the phase function evaluated from Eq. (9). For DL and DM distributions, ν^* is determined by

$$\nu^*=\ln(\tau_{\lambda1}/\tau_{\lambda2})/\ln(\lambda_2/\lambda_1)+2. \quad (10)$$

Table 7. The Phase Functions at $\theta=40°$ Evaluated from Eq. (9) for $m_I=0$

m_R	1.4		1.5		1.6		1.7		Maximum Relative Error (%)
Distribution	P_a	P_a^{**}	P_a	P_a^{**}	P_a	P_a^{**}	P_a	P_a^{**}	
$\nu^*=2$	0.129	0.130	0.137	0.134	0.136	0.135	0.135	0.133	2.2
$\nu^*=3$	0.158	0.162	0.166	0.165	0.167	0.166	0.166	0.164	2.5
$\nu^*=4$	0.173	0.175	0.178	0.178	0.178	0.178	0.175	0.176	1.2
DL($\nu^*=2.43$)	0.143	0.147	0.153	0.151	0.152	0.151	0.151	0.149	2.8
DM($\nu^*=1.98$)	0.127	0.130	0.132	0.133	0.130	0.134	0.126	0.131	3.9

In taking $\lambda_1=550$ nm and $\lambda_2=900$ nm, the values of ν^* in DL and DM distributions determined from Eq. (10) are 2.43 and 1.98, respectively. As shown in Table 7, for Junge distributions with $\nu^*=2$, 3 and 4, and $1.4\leqslant m_R\leqslant 1.7$, the errors of Eq. (9) are less than 2.5%; for non-Junge distributions, the errors are less than 4%. Besides, for these five distributions, when m_R varies from 1.4 to 1.7, the variation of the phase function at $\theta=40°$ is less than 7%, and is also not sensitive to the size distribution. Therefore, under certain distribution and real part of refractive index, the imaginary part of refractive index can be determined from the aerosol phase function at $\theta=40°$ or its weighted phase functions.

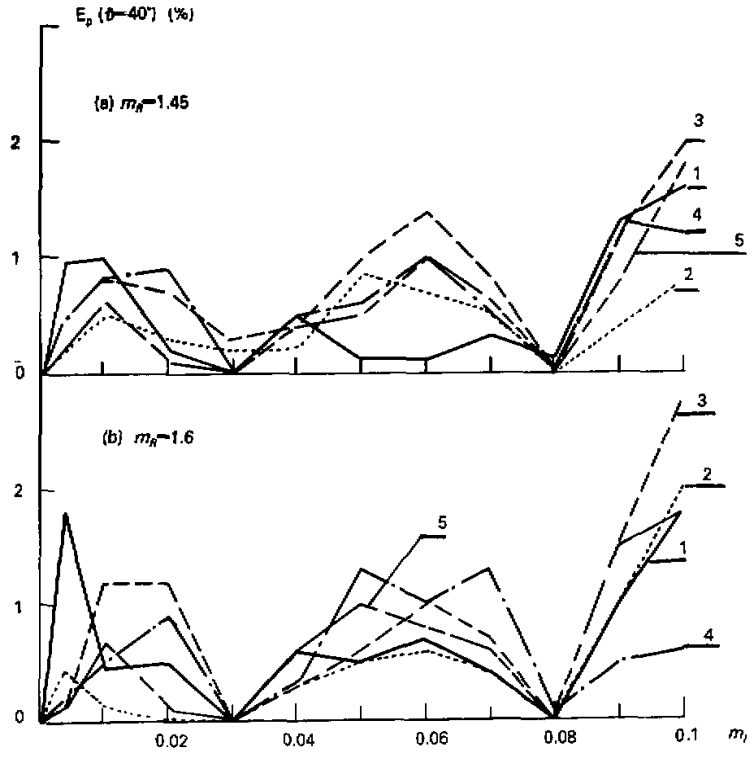

Fig. 2. Relative error of the phase function determined from Eq. (7)
1. $\nu^*=2$; 2. $\nu^*=3$; 3. $\nu^*=4$; 4. DL; 5.DM.

4. *Asymmetric Factor and Single-Scattering Albedo*

Similar to Section 3, by taking 6 grid points, the asymmetric factor can be determined as follows:

$$\begin{cases} g_a = g_a(m_R, m_I = 0) + a_1 m_I^{\{1+10.9E^{0.8m_I}+a_2 m_I^{1.7}} \\ E = 1 - g_a(m_R, m_I = 0.03)/g_a(m_R, m_I = 0)\,. \end{cases} \tag{11}$$

In taking 4 grid points: $m=1.48$—$0.03\,i$, 1.48—$0.08\,i$, 1.54—$0.03\,i$, and 1.54—$0.08\,i$, the single-scattering albedo may be determined as follows:

$$\begin{cases} \tilde{\omega}_a = 1 + a_2 m_I^{\{1+10.9E^{0.8m_I}+a_2 m_I^{1.7}\}}, \\ E = 1 - \tilde{\omega}_a(m_I = 0.03)\,. \end{cases} \tag{12}$$

g_a and $\tilde{\omega}_a$ are less sensitive to the variation of refractive index than the phase function. Thus the Eqs. (11) and (12) are accurate enough.

III. APPLICATION

The above-mentioned approximate equations have been used to process and analyse the experimental data at Luogang airport in Hefei, measured by the radiometer with the

view angle of 1° and five wavelengths of 450 nm, 550 nm, 650 nm, 750 nm and 850 nm. In Table 8 we compare the refractive index and surface albedo evaluated from the approximate formulas with those obtained from the precise solution of radiative transfer equation, the formers denoted by m_R, m_I and A, and the latters m_R^*, m_I^* and A^*. The experimental data in Table 8 were obtained at 8:16 on 17 of November, 1985. As shown in Table 8, the difference in the imaginary part from both approaches is less than 0.0026, and that in m_R is less than 0.03, and that in A, is less than 0.05 . As an average over many measured data, the accuracy of the results from approximate equations will be high, for the average errors of those equations as mentioned previously. are very small.

Table 8. Accuracies of Refractive Index and Surface Albedo Evaluated from Approximated Equations

λ (nm)	τ_a	A^*	A	m_R^*	m_R	m_I^*	m_I
450	0.203	0.103	0.075	1.52	1.54	0.0384	0.0410
550	0.201	0.158	0.190	1.55	1.56	0.0350	0.0349
650	0.184	0.353	0.343	1.49	1.52	0.0342	0.0319
750	0.153	0.325	0.331	1.51	1.51	0.0289	0.0271
850	0.148	0.407	0.454	1.54	1.53	0.0245	0.0227

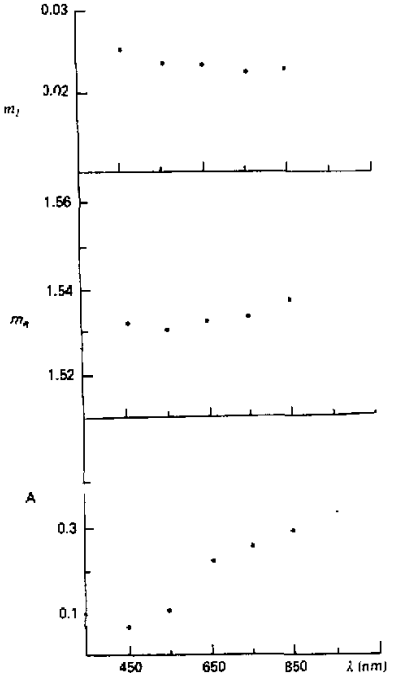

Fig. 3. Mean values of refractive index and surface albedo measured in Hefei.

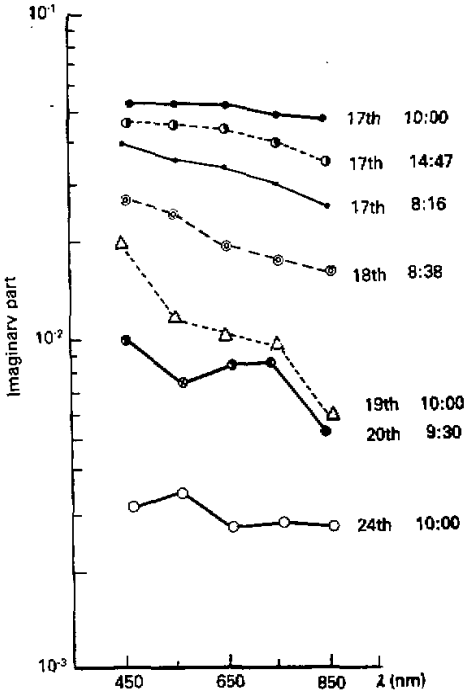

Fig. 4. Imaginary part of refractive index measured at Luogang airport in November, 1985.

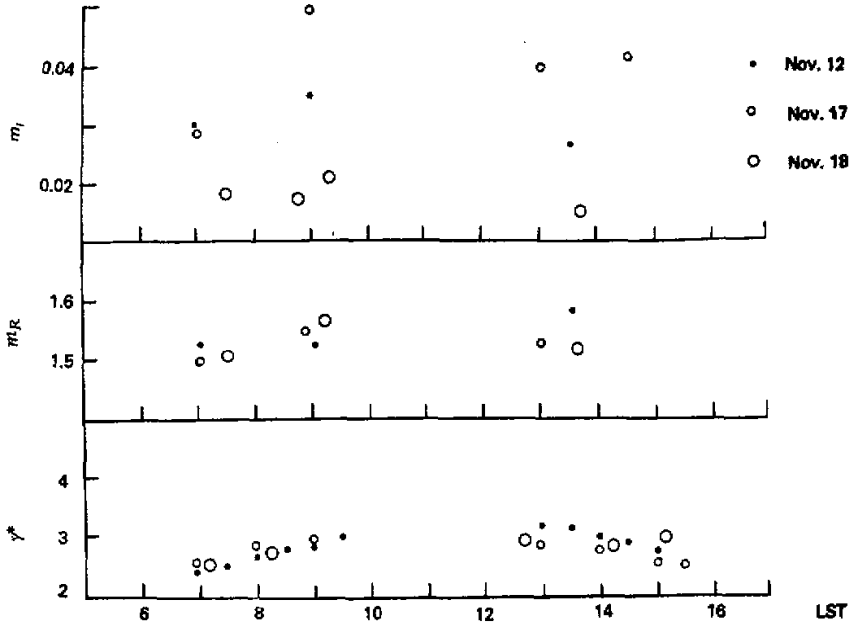

Fig. 5. Diurnal variation of aerosol refractive index and size distribution.

All the following retrieval results are obtained from approximate equations. Fig. 3 shows the mean values of refractive index and surface albedo measured at Luogang in November, 1985. As shown in Fig. 3, the variation of real part of refractive index with wavelength is very small, and its mean value is about 1.53. But as wavelength increases from 450 nm to 850 nm, the imaginary part of refractive index decreases from 0.025 to 0.021, and surface albedo increases greatly from 0.068 to 0.31. By the way, the surrounding Luogang airport is the farmland. According to Kondratyev's study on the albedo for vegetation-covered surface (Kondratyev, 1973), our results seem to be reasonable. Fig. 4 shows the variation of the imaginary part of refractive index with wavelength at different time. During 8 days from 17 to 24 of November, the imaginary part varied from 0.003 to 0.05. The difference in its magnitude was up to one order. Besides, the larger variation was closely dependent upon the weather conditions. During 17–18, November, the imaginary part was larger. However, in the mornings of these two days, the relative humidity was very large, and there was light fog, the imaginary part was smaller than that at any other time in these two days. During 19–20 of November, the cold air flowed over, and dust blowed, the imaginary part decreased and tended to decrease with increasing wavelength. During 22–23, it rained in Hefei. On the first day after raining, or November 24, the imaginary part was the smallest, and was about 0.003. Its variation with wavelength was smaller.

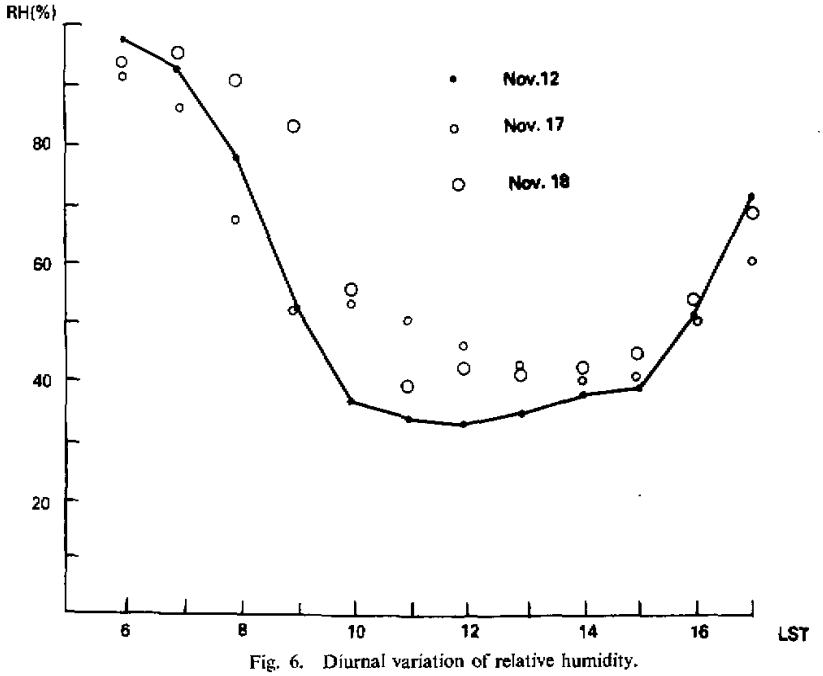

Fig. 6. Diurnal variation of relative humidity.

Fig. 5 shows the diurnal variation of refractive index for 750 nm wavelength and aerosol size distribution. In Fig. 5, ν^* is the fitted Junge distribution parameter from measured optical depth data. During 12 and 17–18 of November, it was obtained that

$2.4 \leqslant \nu^* \leqslant 3.1$, $1.50 \leqslant m_R \leqslant 1.57$ and $0.015 \leqslant m_I \leqslant 0.05$. According to Qiu (1986) et al.'s study the aerosol size distribution in Beijing tends to broaden from morning to afternoon (ν^* decreasing), and the imaginary part decreases. However, there is a different case in Hefei. In the morning, ν^* is generally smaller, large particle is more, and both the real part and the imaginary part of refractive index are small. From morning till noon, ν^* increases, and so do m_R and m_I. In the afternoon, the real part and the imaginary part decrease slightly. This is closely relative to weather conditions. As the relative humidity increases, aerosol particles become large by absorbing vapor. Hence m_R and m_I decrease correspondingly. From Fig. 6 we can see that in the mornings of 12 and 17–18, November, the relative humidity was large, and fog appeared. Thus it seems to be reasonable that ν^*, m_R and m_I in the morning are smaller.

IV. CONCLUSION

Our method for simultaneous determination of aerosol size distribution and its refractive index and surface albedo from the approximate equations of the sky radiance and scattering phase function significantly simplifies the computational process. The inversion errors of the imaginary part of refractive index and surface albedo are estimated to be less than 0.004 and 0.05, respectively. As an average over many data, the errors are smaller.

We have processed the measured data at Luogang airport in Hefei in November, 1985 by using a microcomputer, based on the approximate equations in this paper. We calculate the phase function and single-scattering albedo at grid points. At first, the Mie scattering intensity and extinction factor etc. at grid points are calculated, then they are stored into diskette, and when the phase function at grid points is evaluated, they are read out.

The experimental data showed that under different weather conditions, the variation in the imaginary part of refractive index is rather large. As an average, the real part of refractive index does not vary basically with the increase of wavelength, and its imaginary part changes slightly and surface albedo increases obviously. In the morning, the relative humidity is larger, aerosol particles become larger due to the absorption of moisture, so large particulates increase. Thus the real part and imaginary part of refractive index are relatively smaller.

REFERENCES

Box, M.A. and Deepak, A. (1981), An approximation to multiple scattering in the earth's atmosphere: almucantar radiance formulation, *J. Atmos. Sci.*, **38**:1037–1048.

Kondratyev, K. Ya. (1973), Radiation characteristics of the atmosphere and the earth's surface, Amerind, New Delhi., 580pp.

Qiu Jinhuan and Zhou Xiuji (1986), Simultaneous determination of aerosol size distribution and refractive index and surface albedo from radiance–part I:theory, *Adv. Atmos. Sci.*, **3**:162–171.

Qiu Jinhuan et al. (1986), Simultaneous determination of aerosol size distribution and refractive index and surface albedo from radiance —part II: application, *Adv. Atmos. Sci.*, **3**:341–348.

Tanaka, M., et al. (1982), Simultaneous determination of complex refractive index and size distribution of airborne and water-suspended particle from light scattering measurements, *J. Meteo. Soc. Jap.*, **60**:1259–1272.